Effect of Nanochannel Diameter and Debye Length on Ion Current Rectification in a Fluidic Bipolar Diode

ARTICLE *in* THE JOURNAL OF PHYSICAL CHEMISTRY C · NOVEMBER 2011

Impact Factor: 4.77 · DOI: 10.1021/jp208309g

THE JOURNAL OF PHYSICAL CHEMISTRY C

ARTICLE

pubs.acs.org/JPCC

Effect of Nanochannel Diameter and Debye Length on Ion Current Rectification in a Fluidic Bipolar Diode

Kunwar Pal Singh*,†,‡ and Manoj Kumar‡

†School of Physics, University of Sydney, New South Wales 2006, Australia

‡Singh Simutech Pvt. Ltd., Bharatpur, Rajasthan, 321201, India

Supporting Information

ABSTRACT: We have simulated ion current rectification (ICR) in a bipolar nanochannel fluidic diode for different nanochannel diameters, electrolyte concentrations, and surface charge densities. The ICR decreases with diameter of the fluidic nanochannel due to decrease in unipolar character of the electrolyte. The ICR decreases with electrolyte concentration due to surface charge screening by counterions. The ICR increases with channel diameter for a given ratio of channel diameter to Debye length. Scaling of forward and reverse current densities with electrolyte concentration has been determined using curve fitting for different values of surface charge densities and channel diameters. The ICR can be increased by increasing surface charge density to enhance unipolar character of the electrolyte. The fluid velocity close to the nanochannel walls is driven by body force and along the center by the fluid pressure, which gives rise to a curly fluid flow.

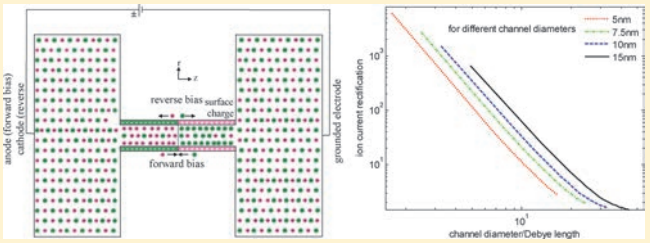

1. INTRODUCTION

Unique transport characteristics are shown by fluidic nanochannels with dimensions comparable to the Debye length due to counterions induced by surface charge. Surface charge effects govern ionic conductance,[1] diffusion,[2] pH-controlled protein transport,[3] and field-effect flow control[4] in nanofluidic devices. A spatial change in the surface charge along the length of a channel results in ionic concentration enhancement, depletion,[5] or both and generation of space charge.[6] Field effect inside a nanofluidic transistor similar to metal-oxide-semiconductor field-effect transistor (MOSFET) can be realized by tailoring spatial distribution of the surface charge along the channel.[7]

Ionic current rectification (ICR) in conical nanopores/nanochannels refers to an asymmetric diode-like current−voltage (*I*-*V*) behavior.[8] Homogeneous silica nanochannels with an ion concentration gradient[9] and conical nanopores with asymmetric geometry produce ICR.[10−12] A pH-dependent electrochemical rectification in a protein ion channel reconstituted on a planar phospholipid membrane was reported. [13] A unipolar diode consists of a charged zone and a neutral zone and a bipolar diode consists of a junction between positively and negatively charged zones of the pore/channel walls. [14,15] A bipolar diode has more asymmetric current−voltage characteristics than a unipolar diode. [16] A linear surface-charge distribution can also produce ionic-current rectification. [17]

The structure of bipolar conical diode is basically the same as the widely investigated bipolar membranes in electrochemistry.[18] A nanofluidic diode possesses similar properties but much smaller size and structure regularity, which may enable it to be integrated on a microfluidic chip to perform pH control, power generation from acidic and basic solutions, and a chemical separation process.[19,20]

Daiguji et al.[20] proposed and modeled a bipolar nanofluidic diode consisting of opposite surface charges on either half of the nanochannel to produce rectification of ion current. The counterions in the fluid induced by surface charge give rise to rectification of ionic current. Fabrication of nanofluidic diodes to create asymmetric surface charges along a nanochannel is a challenging task. Diffusion-limited patterning (DLP) to pattern the cationic protein avidin inside biotinylated nanofluidic channels to modify the surface charge of the nanochannel was developed.[21] Sub-20 nm nanofluidic channels containing positively and negatively charged surfaces were created to form an abrupt junction using distinct isoelectric points of SiO_2 and Al_2O_3 surfaces, and photolithography to define the charge distribution and ion transport behavior was investigated.[22] The effects of size reduction, applied bias, and solution ionic strength were investigated theoretically and numerically in nanochannel based unipolar and bipolar fluidic diodes.[23] Navier−Stokes equations were not included in most of the previous studies[20−22] on nanochannel-based fluidic diode. Scaling of forward and reverse current densities and rectification with electrolyte concentration for different values of surface charge densities and channel diameters is not known. Structure of fluid velocity is also not known from previous works.

Received: June 26, 2011
Revised: October 1, 2011
Published: October 11, 2011

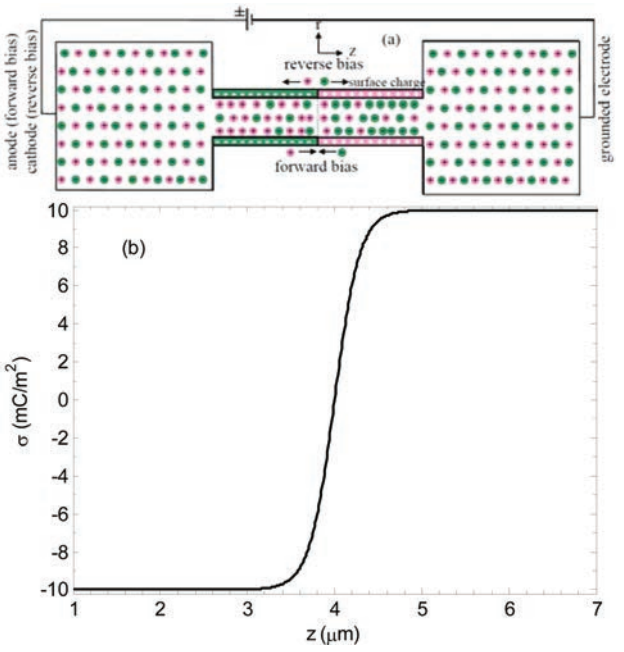

Figure 1. (a) Schematic of bipolar nanochannel fluidic diode. The nanochannel is connected to two identical reservoirs of size 1.0 μm × 1.0 μm filled with a binary electrolyte solution. The length of the nanochannel is 6.0 μm, and the values of diameters are W = 5.0, 7.5, 10, and 15 nm. The location of the nanochannel is from $-w/2$ to $w/2$ nm from z = 1.0 to 7.0 μm. (b) Profile of surface charge density on the walls of the nanochannel.

In this Article, we describe ICR influenced by nanochannel diameter, electrolyte concentration, and surface charge density in a bipolar diode. Scaling of forward and reverse current densities with electrolyte concentration has been determined using curve fitting for different values of surface charge densities and channel diameters. This Article is organized as follows. The next section describes the schematic of bipolar nanochannel diode. Modeling details and code validation are given in Section 3 and the Supporting Information, respectively. Results and Discussion of the simulations are described in Section 4, and summary and conclusions are given in the last section.

2. SCHEMATIC OF BIPOLAR NANOCHANNEL DIODE

Schematic of the bipolar nanochannel diode is shown in Figure 1a. The length of the nanochannel is taken to be 6.0 μm, and different values of nanochannel diameter W are 5.0, 7.5, 10.0, and 15.0 nm to see the effect of diameter on ICR. The nanochannel is connected to two identical reservoirs of size 1 μm × 1 μm filled with a binary electrolyte solution, and the location of the nanochannel is from $r = -W/2$ to $W/2$ nm and z = 1−7 μm. Three-dimensional geometry has been modeled by solving governing equations in two dimensions by using the radial symmetry to reduce numerical complexity. There is negative and positive surface charge on the walls of the channel in left-hand side and right-hand side of the junction, respectively, as shown in Figure 1b. The profile of the surface charge density is given by following equation.

$$\sigma = \sigma_0\left(\frac{2}{1 + \exp[-k(z - z_0)]} - 1\right) \quad (1)$$

where σ_0 is the peak value of the surface charge density, z_0 is the location of the junction, and k is associated with the width of the transition zone. As the value of k increases, sharpness of the profile increases and width of transition zone decreases. The value of k is taken to be 10 μm^{-1} in our simulations.

The polarity of the counterions depends on the type of surface charge on the walls of the nanochannel. Negative surface charge induces cation majority carriers in the channel and vice versa. The net concentration of the counterions in a nanochannel is governed by electroneutrality and depends on the surface charge density σ on the nanochannel walls. The electroneutrality condition plays an important role in fluidic nanochannels. From the requirement of overall electroneutrality, the relation between the difference in ionic concentrations $(n_+ - n_-)$ and surface charge density is given by[24]

$$(n_+ - n_-) = -\frac{2\sigma}{ew} \quad (2)$$

where e is electron charge. Applying voltage of one polarity (forward bias) allows flow of the ions from the bulk solutions, and steady flow of the current is observed. An opposite polarity (reverse bias) causes the ions to move away from the junction and out of the nanochannel. Because there is no source close to the junction, ions cannot be replenished. An ion-depleted region is created close to the junction, leading to negligible flow of ion current.

3. MODELING DETAILS

The continuum description of ion transport by the PNP equations can successfully predict the main properties of many biological channels. Other computational methods like Brownian dynamics are more precise but computationally too expensive. The continuum approach has a clear advantage in terms of computational time and thus improvement in design. The validity of the mean-field approximation in PNP theory was tested by comparing its predictions with those of Brownian dynamics simulations in cylindrical channels and in a realistic potassium channel. It was found that the continuum description of ion transport by the PNP equations produces correct results validating the physical and chemical phenomena occurring inside a nanochannel with diameter bigger than approximately 2D lengths for the ionic species.[25]

For nanofluidic channels with dimensions smaller than the characteristic length scale for ion screening known as Debye length (λ_D), overlapping of electric double layers of charged channel walls results in a unipolar solution of counterions. We define inverse Debye length by following relation[26]

$$k_D = \left(\frac{2e^2 n_b}{\varepsilon_0 \varepsilon_r k_B T}\right)^{1/2} \quad (3)$$

where n_b is bulk electrolyte concentration, ε_0 is the permittivity of vacuum, ε_r is relative dielectric constant, and T is the absolute temperature in Kelvin. We have taken ε_r = 80 and temperature T = 295 K.

The validity of continuum description of ion transport by the PNP equations becomes an issue for narrow channels at low electrolyte concentrations. The smallest diameter is 5 nm and electrolyte concentration n_b = 10 mM for the cases considered by us. The value of Debye length turns out to be nearly 3 nm. We can conclude that the continuum description of ion transport by

the PNP equations will remain approximately valid for these parameters. Recently, simulation models based on Poisson−Nernst−Planck (PNP) equations has been used to predict the ICR behavior in nanopores, and it was determined that it can validate experimental results.[27,28]

The dynamics of the ions in the system is governed by the PNP equations given as follows

$$\nabla \cdot \mathbf{j}_{\pm} = 0 \tag{4}$$

$$\varepsilon_0 \varepsilon_r \nabla^2 \phi = -e(n_+ - n_-) \tag{5}$$

The electric field associated with the potential is given by following

$$\mathbf{E} = -\nabla \phi$$

The current fluxes associated with the ions are given as follows

$$\mathbf{j}_{\pm} = \mathbf{u} n_{\pm} \pm n_{\pm} \mu_{\pm} \mathbf{E} - D_{\pm} \nabla n_{\pm} \tag{6}$$

where D_+ and D_- are the diffusion coefficients of positive and negative ions, respectively. We have considered constant values for the diffusion coefficients throughout the volume of the system, $D_+ = 1.95 \times 10^{-9}$ m^2/s and $D_- = 2.03 \times 10^{-9}$ m^2/s corresponding to KCl solution.[28,29] The mobilities of the ions are calculated by $\mu_+ = eD_+/k_BT$ and $\mu_- = eD_-/k_BT$, where k_B is the Boltzmann constant and the fluid velocity is given by $\mathbf{u} = \hat{X}u + \hat{y}v$.

Fluid dynamics is governed by continuity equation and Navier−Stokes equations. The continuity equation and the Navier−Stokes equation for incompressible viscous fluids are as follows

$$\nabla \cdot \mathbf{u} = 0 \tag{7}$$

$$\rho\left(\frac{\partial \mathbf{u}}{\partial t} + (\mathbf{u} \cdot \nabla)\mathbf{u}\right) = -\nabla p + \eta \nabla^2 \mathbf{u} + e(n_+ - n_-)\mathbf{E} \tag{8}$$

where η is the viscosity, ρ is the fluid density, and p is the pressure.

Boundary conditions are as follows:

At nanochannel walls

$$\mathbf{n} \cdot \mathbf{j}_{\pm} = 0, \ \mathbf{n} \cdot \nabla \phi = -\frac{\sigma}{\varepsilon_r \varepsilon_0}, \text{ and } u = 0 \tag{9}$$

At reservoir walls

$$\nabla n_{\pm} = 0, \quad \nabla \phi = 0, \quad \nabla p = 0, \quad \text{and} \quad \mathbf{u} = 0 \tag{10}$$

At electrodes

$$n_{\pm} = n_b, \ \phi = 0 \text{ (groundedelectrode)}, \quad \phi = V_0 \text{ (cathodeoranode)}, \ p = 0, \text{ and } \nabla \mathbf{u} = 0 \tag{11}$$

The self-consistent formulation consisting of governing equations and boundary conditions given by eqs 4−11 is solved using a Galerkin variational formulation-based finite-element method.[30,31] We validated accuracy of the numerical code used to evaluate ion currents for two problems involving electrical double layer adjacent to a flat surface and electro-osmotic (EOF) in a nanochannel for which analytical solutions exist. Code validation is described in the Supporting Information. Having verified the code, the next step is to apply it to the computation of the ion concentrations, potential distributions, and fluid velocity for bipolar diode with different nanochannel diameters to investigate effect of nanochannel diameter and Debye length on ICR in a fluidic bipolar diode.

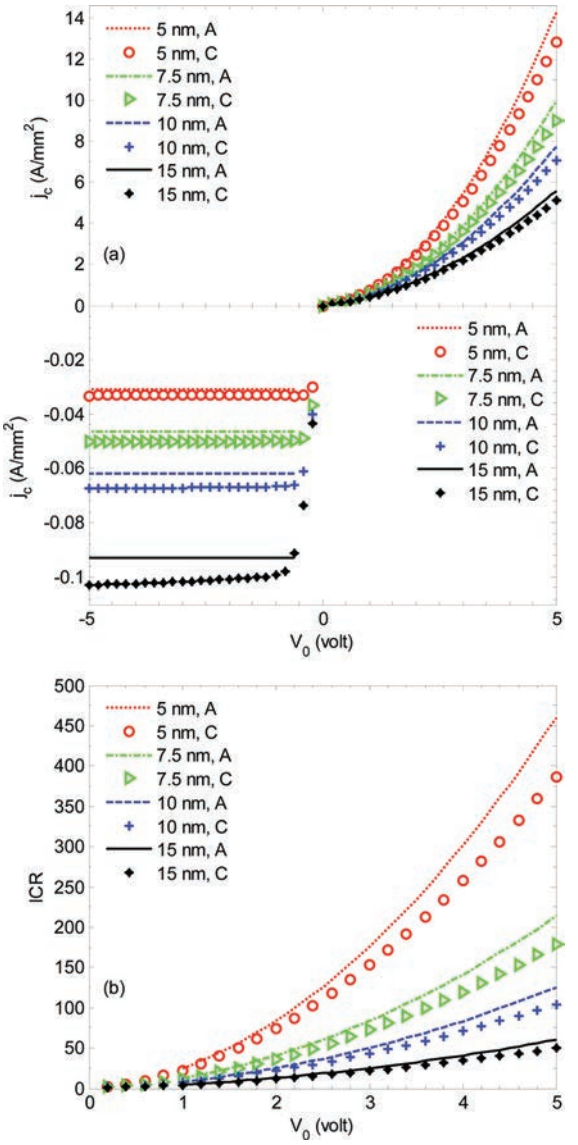

Figure 2. (a) Ion current density as a function of potential across the nanochannel and (b) corresponding ICR ratio as a function of absolute potential for electrolyte concentration n_b = 100 mM, and surface charge density σ_0 = 10 mC/m^2. Different lines are for analytical solutions and symbols are for computational solutions for channel diameters w = 5, 7, 10, and 15 nm. Analytical value of ion current density for forward as well as reverse bias has been multiplied by a factor of 2 in the plots.

4. RESULTS AND DISCUSSION

The motion of the ions is toward each other as well as toward junction under the influence of the applied electric field. The ions cross the junction, which allows smooth flow of the ions from the bulk solutions, and steady flow of the current. This leads to increase in ion concentrations in the nanochannel with increasing electrolyte concentrations. Higher electrolyte concentration screens the effect of surface charge on the walls of the nanochannel. Lower effective surface charge and higher ionic concentrations lead to the increase in the electrostatic force between opposite ion, and the profiles of the positive and negative ions become

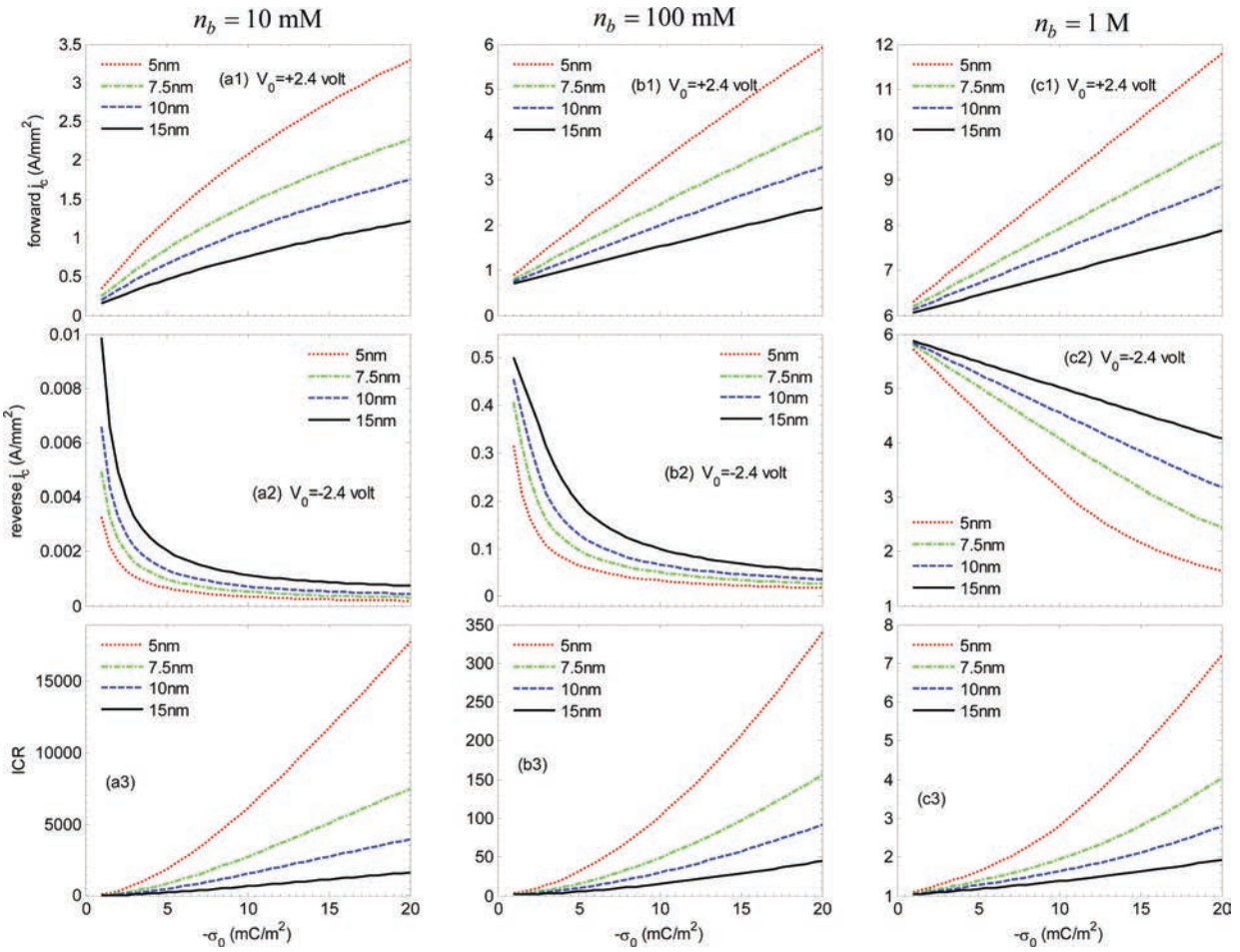

Figure 3. Forward ion current density at V_0 = +2.4 V, reverse ion current at V_0 = −2.4 V, and ICR as a function of surface charge density on the walls of the nanopore. The figures with prefix a−c are for three different values of electrolyte concentrations c_{b1} =10 mM, c_{b2} = 100 mM, and c_{b3} =1 M, respectively. Different lines are for channel diameters w = 5, 7.5, 10, and 15 nm.

similar to each other. The concentration of ion species decreases with nanochannel diameter due to decrease in the value of excess charge with channel diameter to maintain electroneutrality. Positive ions move toward left and negative ions toward right, that is, away from the junction or from nanochannel to the reservoirs for reverse bias. Because there is no source close to the junction, ions cannot be replenished, and an ion-depleted region is created close to the junction. Different lines in the Figures in the following description are for channel diameters w = 5, 7.5, 10, and 15 nm.

4.1. Ion Current Rectification. It is important to investigate the effect of applied potential, surface charge density, and electrolyte concentration on ICR for different nanochannel diameters. In this subsection, the effect of these parameters on ICR has been investigated.

4.1.1. Effect of Applied Potential. Analytical expressions relating applied potential and ion current have been derived in previous studies using 1D PNP equations.[22,23,32,33] We can write following equations using ref 22.

At large forward biases, forward ion current density can be approximated to following

$$J_F = D\frac{\sigma_0}{4wL}\left(4\sqrt{1+\left(\frac{ewn_b}{\sigma_0}\right)^2}\frac{e}{k_bT}V_0 + \left(\frac{e}{k_bT}V_0\right)^2\right) \quad (12)$$

The reverse ion current density saturates to following value

$$J_{sat} = -\frac{Dew}{\sigma_0 L}n_b^2 \quad (13)$$

where we have taken diffusion coefficient $D = 2 \times 10^{-9}$ m^2/s.

Figure 2a,b shows ion current density and corresponding ICR as a function of potential across the nanochannel. Analytical and computational curves are shown for comparison after multiplying analytical value of ion current density (for forward as well as reverse bias) by a factor of 2. The device is forward biased for positive values of V_0 and reverse biased for negative values of V_0 as previously mentioned. The current density increases with applied potential of forward bias and decreases with diameter of the nanochannel. We determined (not shown) that the concentration of ion species decreases, and there was no significant change in the electric field with an increase in the diameter of the nanochannel. Hence, the current density decreases with channel diameter for forward bias. Reverse current density increases with channel diameter. A good agreement between analytical and computed values can be seen from the Figure after multiplying analytical values by a factor of 2.

Analytical values of reverse saturation current are equal to each other in refs 22 and 23. They determined that analytical value of the current is underestimated by a factor of ∼2 during reverse

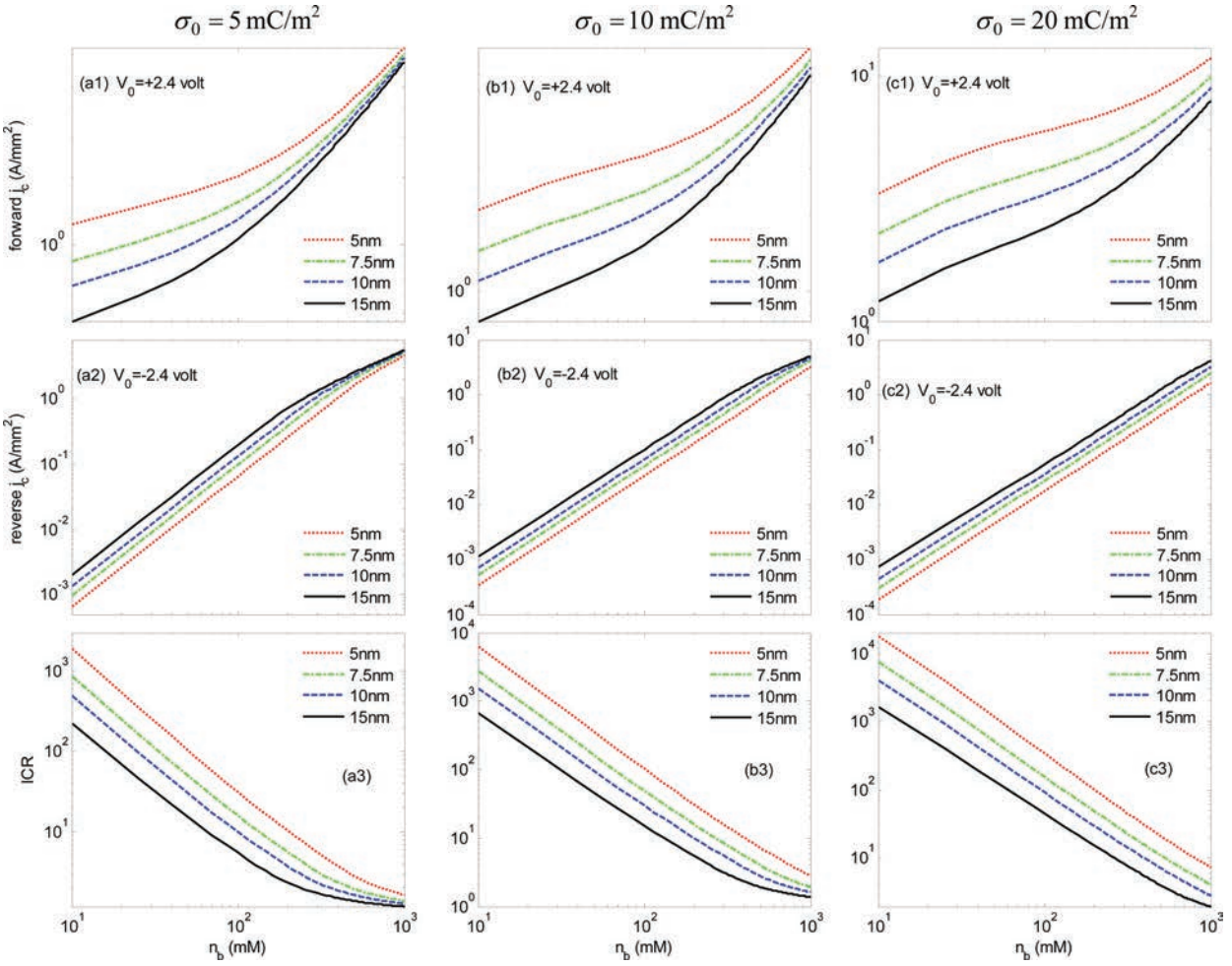

Figure 4. Forward ion current density at $V_0 = +2.4$ V, reverse ion current at $V_0 = -2.4$ V, and ICR as a function of electrolyte concentration. The Figures with prefix a−c are for three different values of surface charge density on the walls of the nanopore $\sigma_0 = 5.0$, 10.0, and 20.0 mC/m^2. Different lines are for channel diameters $w = 5$, 7.5, 10, and 15 nm.

bias, which may be related to the breakdown current in reverse bias[22] or shortcomings of the 1D Donnan equilibrium treatment in predicting the minority carrier concentration in nanopores.[23] However, we determine that analytical derivations in ref 22 underestimate ion current density for forward as well as reverse bias at high applied potentials by a factor of 2. The factor 2 may have missed in analytical derivations in ref 22 due to assumptions used in their study. The junction between oppositely charged zones was assumed sharp in analytical derivations. A finite width of the junction leads to lower values of computed forward current and higher values of reverse current than the analytical values.

Figure 2b shows corresponding ICR in the nanochannel as a function of absolute value of anode potential. ICR is obtained by using values in the Figure 2a, by dividing forward current density with reverse current density at the same potential. The variation of the ratio with channel diameter is dictated by the value of current for reverse bias. It can be seen that ICR is nearly 385 at 5 V for $n_b = 100$ mM and channel diameter 5 nm. Lowest value of current rectification at 5 V is nearly 50 for $n_b = 100$ mM and channel diameter 15 nm. Lower values of computed forward current and higher values of reverse current lead to lower computed ICR than the analytical values.

4.1.2. Effect of Surface Charge Density. The surface charge density is one of the key factors to influence ICR. Figure 3a−c shows forward ion current density, reverse ion current density, and corresponding ICR as a function of surface charge density σ_0. Figures with suffixes 1−3 are for electrolyte concentration n_b = 10, 100, and 1.0 M, respectively. We found that concentration of ions increases with surface charge density and the electric field decreases. Increase in the concentration dominates the decrease in the electric field, which leads to overall increase in the forward current with surface charge density. The unipolar character of the electrolyte in both zones increases with an increase in surface charge density which leads to enhanced ion depletion for reverse bias and reduced reverse current. The rectification increases rapidly with surface charge density due to combined effect of increase in forward current and decrease in reverse current. It can be seen that ICR approaches nearly 335 for surface charge density σ_0 = 20 mC/m^2 and electrolyte concentration 100 mM for nanochannel diameter 5 nm.

4.1.3. Effect of Electrolyte Concentration. Figure 4 shows forward ion current density at $V_0 = +2.4$ V, reverse ion current density at $V_0 = -2.4$ V, and corresponding ICR, respectively, as a function of bulk electrolyte concentration. The figures with suffixes 1−3 are for surface charge density $\sigma_0 = 5$ mC/m^2 σ_0 = 10 mC/m^2 and $\sigma_0 = 20$ mC/m^2, respectively. A higher number of ions can flow from the reservoirs to nanochannel under the

dx.doi.org/10.1021/jp208309g |*J. Phys. Chem. C* 2011, 115, 22917–22924

Table 1. Fitting Parameters for the Relation between Current Density (A/mm^2) and Bulk Electrolyte Concentration (mM), $j_c = \alpha + \beta n_b^{\gamma}$, for the curves shown in Figure 4

		forward bias			reverse bias		
σ_0 (mC/m^2)	w (nm)	$\alpha \times 10$	$\beta \times 10^3$	γ	$\alpha \times 10$	$\beta \times 10^5$	γ
5.0	5.0	13.2	8	0.96	1.21	−15	1.5
	7.5	8.85	7.2	0.98	1.87	−76	1.28
	10.0	6.64	6.77	0.98	2.11	−158	1.18
	15.0	4.43	6.43	0.99	2.11	−300	1.09
10.0	5.0	24.14	15.78	0.87	0.065	−0.44	1.95
	7.5	16.36	10.97	0.92	0.62	−3.3	1.70
	10.0	12.4	9.21	0.94	1.20	−15.6	1.50
	15.0	8.31	7.78	0.96	1.86	−76.6	1.28
20.0	5.0	3.82	0.103	0.63	−7.7	−0.183	1.98
	7.5	2.75	0.039	0.75	−0.0016	−0.275	1.98
	10.0	2.14	0.014	0.82	0.0044	−0.472	1.94
	15.0	1.47	0.014	0.88	0.06	−3.45	1.70

influence of electric field with increasing electrolyte concentration which leads to increase in concentration of ions in the channel and increase in the forward current density. The accumulation of counterions close to the nanochannel walls screens effect of surface charge, which leads to reduced unipolar character of electrolyte in two segments of the diode and an increase in the reverse current density. Both forward as well as reverse ion current densities increase with electrolyte concentration with different slops. The ICR decreases rapidly with electrolyte concentration due to increase in reverse current density which dominates increase in the forward current density.

Cheng and Guo[22] determined experimentally that both forward ion current and reverse ion current increase with electrolyte concentration above 1 mM and ICR decreases monotonically in a bipolar diode. Our findings are consistent with their results. Vlassiouk et al.[23] found numerically that ICR decreases monotonically with electrolyte concentration in a bipolar diode and peaks for an intermediate value of concentration. Previous experimental[34] and numerical[35] studies on the effect of nanopore geometry on ICR in a unipolar diode determined that ICR peaks for intermediate value of concentration. We can conclude that trend of change of ICR with electrolyte concentration is different in bipolar and unipolar diodes.

Nonlinear curve fitting has been used to find scaling of forward and reverse current densities with electrolyte concentration for different nanochannel diameters and surface charge densities for the results in Figure 4. Different curves can be approximately fitted using relation $j_c = \alpha + \beta n_b^{\gamma}$, where j_c is current density in A/mm^2, α, β and γ are fitting constants, and n_b is electrolyte concentration in mM. Table 1 shows values of fitted parameters for different curves shown in Figure 4. The values of γ for forward current density vary from 0.96 to 0.99, 0.87 to 0.96, and 0.63 to 0.88 for surface charge densities $\sigma_0 = -5, -10$, and -20 mC/m^2, respectively, for the nanochannel diameters in increasing order. The corresponding values of γ for reverse current densities are 1.5 to 1.09, 1.95 to 1.28 and 1.98 to 1.7. As the value of surface charge density decreases or nanochannel diameter increases the value to γ tends to 1, indicating that current density tends to increase linearly with electrolyte concentration for low values of surface charge density, higher values of channel diameters, or both.

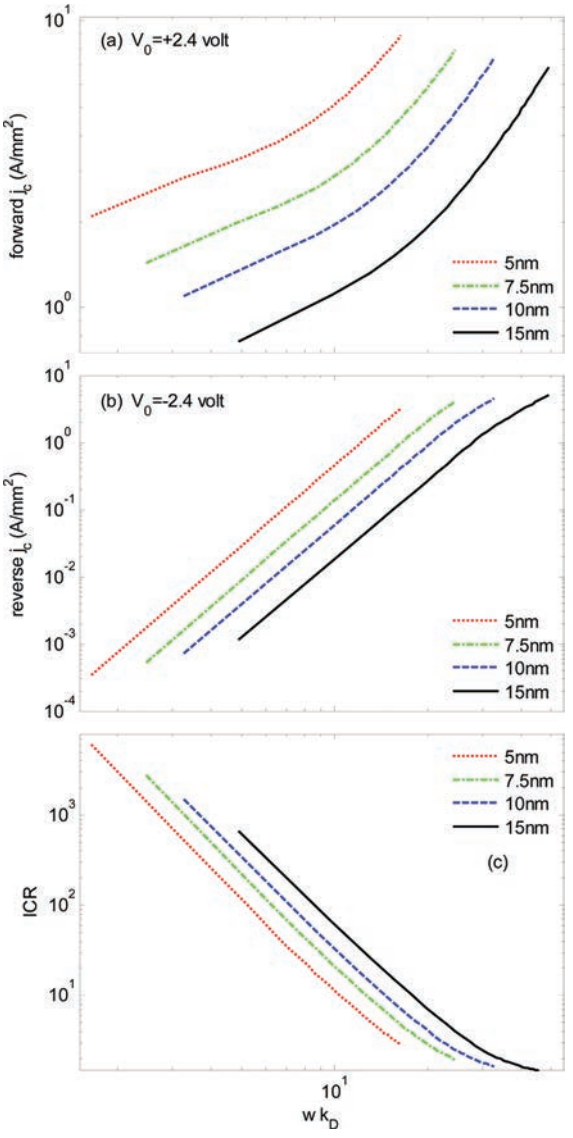

Figure 5. Forward ion current density at $V_0 = +2.4$ V, reverse ion current at $V_0 = -2.4$ V, and ICR as a function of ratio of channel diameter to Debye length for surface charge density $\sigma_0 = 10.0$ mC/m^2. Different lines are for channel diameters $w = 5$, 7.5, 10, and 15 nm.

Forward ion current density at $V_0 = +2.4$ V, reverse ion current density at $V_0 = -2.4$ V, and corresponding ICR as a function of ratio of channel diameter to Debye length are shown in Figure 5a−c for surface charge density $\sigma_0 = 10.0$ mC/m^2. It can be seen that ICR decreases with the ratio of channel diameter to Debye length due to decrease in unipolar character of electrolyte as previously stated. The ICR increases with channel diameter for a given ratio of channel diameter to Debye length due to relatively higher increase in the forward current density.

4.2. Fluid Velocity. It is interesting to see structure of fluid velocity in the nanochannel. We describe distribution of the fluid velocity inside the nanochannel in this subsection. Vectors of electrolyte velocity in the nanopore are shown in Figure 6a for forward bias at $V_0 = +2.4$ V and in Figure 6b for reverse bias at $V_0 = -2.4$ V for nanochannel diameter $W = 10$ nm at electrolyte concentration $n_b = 100.0$ mM. Electrolyte velocity is induced by body force $e(n_i - n_e)\mathbf{E}$ which is a product of excess charge and

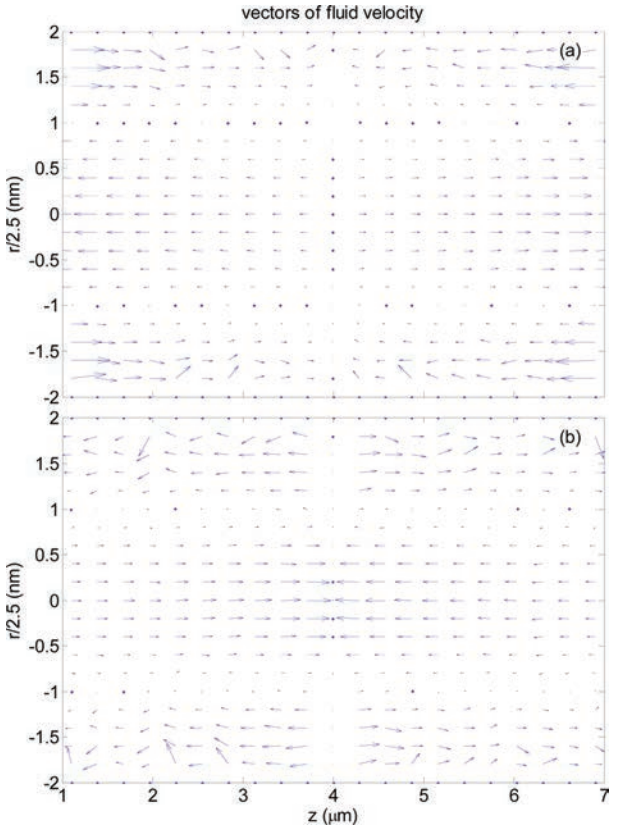

Figure 6. Vectors of fluid velocity in the nanochannel for (a) forward bias at V_0 = +2.4 V and (b) reverse bias at V_0 = −2.4 V for surface charge density σ_0 =10 mC/m^2, electrolyte concentration n_b = 100.0 mM, and nanochannel diameter w = 10 nm.

electric field. The fluid velocity close to the walls is the positive z direction in the left zone and negative z direction in the right zone for forward bias. The fluid velocity for reverse bias is in the opposite direction as that for forward bias. The velocity of the electrolyte along the center of the nanochannel is in the opposite direction to the velocity close to the walls for both biases. The fluid enters the nanochannel through close to the walls under the influence of body force and then exits though the center of the channel during forward bias. The fluid exits the nanochannel from close to the walls under the influence of body force and it enters through the center of the channel during reverse bias. Opposite fluid velocities close to the center and close to the walls of the nanochannel give rise to curly fluid flow between center and the walls of the channel. The fluid entering or exiting the nanochannel close to the walls under the influence of body force generates fluid pressure that drives the fluid at the center for forward as well as reverse bias. The fluid velocity peaks close to the entrance (at $z = 1\ \mu$m) and exit (at $z = 7\ \mu$m) of the nanochannel for forward bias. The fluid velocity peaks close to the junction (around $z = 4\ \mu$m) for reverse bias. The fluid velocity changes its direction as we move from the center of the nanochannel toward the walls for forward bias as well as reverse bias. The magnitude of body force depends on the electric field and net ion concentration, which is dictated by electroneutrality. The magnitude and direction of fluid velocity is jointly influenced by body force and fluid pressure. We determined that the magnitude of the velocity for reverse bias is small as compared with the velocity for forward bias.

We calculated (not shown) ICR with and without electro-osmotic flow and determined that there was negligible difference between two results. The contribution of electro-osmotic flow from oppositely charged zones cancel each other because of opposite fluid flows close to the walls. Even though noninclusion of Navier−Stokes equations does not make much difference, their inclusion in the modeling is necessary considering findings in refs 36 and 37 that electro-osmotic flow may have significant effect on ion transport in uniformly charged nanochannels or nanopores. Furthermore, we cannot find out about cancellation of electro-osmotic flow without including Navier−Stokes equations in the modeling.

5. SUMMARY AND CONCLUSIONS

We have investigated ICR in a nanofluidic bipolar diode for different nanochannel diameters, electrolyte concentrations and surface charge densities. The ions enter the nanochannel from reservoirs during forward bias enriching the channel, leading to smooth flow of the ion current. The motion of the ions is from the nanochannel to the reservoirs during reverse bias, creating ion depletion in the nanochannel that leads to negligible flow of ion current during reverse bias. The ICR decreases with the diameter of the fluidic nanochannel due to reduced unipolar character of electrolyte, which can be increased/compensated by increasing surface charge density to enhance ICR. The ICR decreases with electrolyte concentration due to screening of the surface charge, reduction in unipolar character of electrolyte, and increase in reverse current. The ICR increases with channel diameter for a given ratio of channel diameter to Debye length. Our numerical results are in good agreement with previously reported analytical and experimental results. Scaling of forward and reverse current densities with electrolyte concentration has been determined. The fluid velocity close to the nanochannel walls is driven by body force and along the center by the fluid pressure, which leads to fluid entering the nanochannels along the walls for forward bias and along the center of the nanochannel for reverse bias.

■ ASSOCIATED CONTENT

Ⓢ Supporting Information. We validated the accuracy of the numerical code used in this Article to evaluate ion currents for two problems involving electrical double layer adjacent to a flat surface and electro-osmotic (EOF) in a nanochannel for which analytical solutions exist. This material is available free of charge via the Internet at http://pubs.acs.org.

■ AUTHOR INFORMATION

Corresponding Author
*E-mail: k_psingh@yahoo.com.

■ ACKNOWLEDGMENT

This work was supported and the code used in this work was developed by Singh Simutech Pvt. Ltd., Bharatpur, Rajasthan, India.

■ REFERENCES

(1) Stein, D.; Kruithof, M.; Dekker, C. *Phys. Rev. Lett.* **2004**, *93*, 035901.
(2) Plecis, A.; Schoch, R. B.; Renaud, P. *Nano Lett.* **2005**, *5*, 1147–1155.

(3) Schoch, R. B.; Bertsch, A.; Renaud, P. *Nano Lett.* **2006**, *6*, 543–547.
(4) Karnik, R.; Castelino, K.; Majumdar, A. *Appl. Phys. Lett.* **2006**, *88*, 123114.
(5) Pu, Q.; Yun, J.; Temkin, H.; Liu, S. *Nano Lett.* **2004**, *4*, 1099–1103.
(6) Wang, Y. C.; Stevens, A. L.; Han, J. Y. *Anal. Chem.* **2005**, *77*, 4293–4299.
(7) Karnik, R.; Fan, R.; Yue, M.; Li, D. Y.; Yang, P. D.; Majumdar, A. *Nano Lett.* **2005**, *5*, 943–948.
(8) Cheng, L.- J.; Guo, L. J. *Nano Lett.* **2007**, *7*, 3165–3171.
(9) Jung, J. Y.; Joshi, P.; Petrossian, L.; Thornton, T. J.; Posner, J. D. *Anal. Chem.* **2009**, *81*, 3128–3133.
(10) Siwy, Z. S. *Adv. Funct. Mater.* **2006**, *16*, 735–746.
(11) Woermann, D. *Phys. Chem. Chem. Phys.* **2004**, *6*, 3130–3132.
(12) Cruz-Chu, E. R.; Aksimentiev, A.; Schulten, K. *J. Phys. Chem. C* **2009**, *113*, 1850–1862.
(13) Alcaraz, A.; Ramirez, P.; Garcia-Gimenez, E.; Lopez, M. L.; Andrio, A.; Aguilella, V. M. *J. Phys. Chem. B* **2006**, *110*, 21205–21209.
(14) Vlassiouk, I.; Siwy, Z. S. *Nano Lett.* **2007**, *7*, 552–556.
(15) Yan, R.; Liang, W.; Fan, R.; Yang, P. *Nano Lett.* **2009**, *9*, 3820–3825.
(16) Nguyen, G.; Vlassiouk, I.; Siwy, Z. S. *Nanotechnology* **2010**, *21*, 265301.
(17) Qian, S.; Joo, S. W.; Ai, Y.; Cheney, M. A.; Hou, W. *J. Colloid Interface Sci.* **2009**, *329*, 376–383.
(18) Hurwitz, H. D.; Dibiani, R. *J. Membr. Sci.* **2004**, *228*, 17–43.
(19) Nagarale, R. K.; Gohil, G. S.; Shahi, V. K. *Adv. Colloid Interface Sci.* **2006**, *119*, 97–130.
(20) Daiguji, H.; Oka, Y.; Shirono, K. *Nano Lett.* **2005**, *5*, 2274–2280.
(21) Karnik, R.; Duan, C. H.; Castelino, K.; Daiguji, H.; Majumdar, A. *Nano Lett.* **2007**, *7*, 547–551.
(22) Cheng, L.-J.; Guo, L. J. *ACS Nano* **2009**, *3*, 575–84.
(23) Vlassiouk, I.; Smirnov, S.; Siwy, Z. S. *ACS Nano* **2008**, *2*, 1589–1602.
(24) Cervera, J.; Alcaraz, A.; Schiedt, B.; Neumann, R.; Ramirez, P. J. *Phys. Chem. C* **2007**, *111*, 12265–12273.
(25) Corry, B.; Kuyucak, S.; Chung, S. H. *Chem. Phys. Lett.* **2000**, *320*, 35–41.
(26) Probstein, R. F. *Physicochemical Hydrodynamics: An Introduction*; Wiley: New York, 1994.
(27) Constantin, D.; Siwy, Z. S. *Phys. Rev. E* **2007**, *76*, 041202.
(28) Hille, B. *Ion Channels of Excitable Membrane*, 3rd ed.; Sinauer Associates: Sunderland, MA, 2001.
(29) Robinson, R. A.; Stokes, R. H. *Electrolyte Solutions*; Butterworth: London, 1955.
(30) Singh, K. P.; Roy, S. *J. Appl. Phys.* **2007**, *101*, 123308.
(31) Singh, K. P.; Roy, S. *Appl. Phys. Lett.* **2008**, *92*, 111502.
(32) Sokirko, A. V.; Ramirez, P.; Manzanares, J. A.; Mafe, S. *Phys. Chem. Chem. Phys.* **1993**, *97*, 1040–1049.
(33) Mafe, S.; Ramirez, P. *Acta Polym.* **1997**, *48*, 234–250.
(34) Apel, P. Y.; Blonskaya, I. V.; Orelovitch, O. L.; Ramirez, P.; Sartowska, B. A. *Nanotechnology* **2011**, *22*, 175302.
(35) Ramirez, P.; Apel, P. Y.; Cervera, J.; Mafe, S. *Nanotechnology* **2008**, *19*, 315707.
(36) Daiguji, H.; Yang, P. D.; Majumdar, A. *Nano Lett.* **2004**, *4*, 137–142.
(37) Ai, Y.; Zhang, M.; Joo, S. W.; Cheney, M. A.; Qian, S. *J. Phys. Chem. C* **2010**, *114*, 3883–3890.